Time-dependent diffusion and annihilation of positrons implanted in a semi-infinite medium

1991 J. Phys.: Condens. Matter 3 681

(http://iopscience.iop.org/0953-8984/3/6/006)

J. Phys.: Condens. Matter 3 (1991) 681–692. Printed in the UK

Time-dependent diffusion and annihilation of positrons implanted in a semi-infinite medium

D T Britton
Universität der Bundeswehr München, Institut für Nukleare Festkörperphysik, D-8014 Neubiberg, Federal Republic of Germany

Received 23 April 1990, in final form 12 October 1990

Abstract. Annihilation spectra, resulting from the implantation of mono-energetic positrons in a perfect homogeneous solid, have been modelled allowing for the transport of both thermal and epithermal positrons. The resulting curves resemble a sum of two exponential components, although the intensities are not simply related to the positron back-diffusion probability. Because of the very short times involved, the effects of non-thermal positron transport are less significant than for steady-state diffusion models. At room temperature, internal reflection of thermal positrons at the surface has little effect on the solution to the diffusion equation for deeply implanted positrons.

1. Introduction

The motion and subsequent escape or annihilation of positrons implanted into a homogeneous defect-free solid are well described by a one-dimensional diffusion equation [1]

$$D\,\partial^2 u/\partial z^2 - \lambda u(z,t) = \partial u/\partial z \tag{1}$$

where D is the diffusion coefficient and z the depth inside the material. Positrons can be lost from the system at the surface or by annihilation, determined by the decay rate λ.

In traditional positron beam experiments, mono-energetic positrons are implanted in a sample and the total fraction diffusing back to the surface is measured, either directly or from the fraction of positronium (Ps) formed. Alternatively the characteristic annihilation lineshape parameter is measured and taken to be a weighted superposition of bulk and surface values. The different experimental and analytical methods are extensively covered in a recent review by Schultz and Lynn [2], and only the relevant details are presented here. In these cases the measurement is averaged over the life of the positrons and a steady-state diffusion equation

$$D\,\partial^2 u/\partial z^2 - \lambda u(z) + P(z) = 0 \tag{2}$$

can be applied. Here $P(z)$ is a time-averaged source of positrons, normally taken as the positron implantation profile which is well known from both experiment [3] and Monte

0953-8984/91/060681 + 12 $03.50

Carlo simulations [4] to be very nearly the derivative of a Gaussian with an energy-dependent range x_0. For a perfectly absorbing surface, the probability that a positron escapes from the sample is simply the Laplace transform of the implantation profile

$$J = \int_0^\infty P(z) \exp\left(-\frac{z}{L}\right) dz. \tag{3}$$

The transform variable is the inverse of the positron diffusion length L, which is related to the diffusion coefficient and bulk annihilation rate by $L^2 = D/\lambda$. The probability of forming Ps or the contribution to the surface lineshape parameter is then simply proportional to J.

In bulk positron annihilation studies, one of the most useful parameters to study is the positron lifetime, which is very sensitive to different material conditions. This has led to the relatively recent development of time-resolved low-energy positron beams such as the RF pulsed beam at Munich [5]. Another method is to use the secondary electrons emitted as the positron impinges on the sample as a start signal for a timing spectrometer [6]. However, in calculating the contribution of the different surface process to the lifetime spectrum, the full time-dependent diffusion equation must be solved. Frieze *et al* [7] have presented a solution for the case of thermal positrons implanted in a solid which describes the essential effects of diffusion on the lifetime spectrum. The present work builds on this, to consider two effects which have recently been recognized as significant in steady-state measurements. These are internal reflection of the positron wavefunction at the surface [8] and the contribution of unthermalized positrons reaching the surface at low implantation energies [9]. Unlike the earlier work, trapping at bulk defects is not considered.

2. Diffusion and annihilation of positrons

The observed positron lifetime spectrum is a superposition of the annihilation rates from all possible states, where each partial component is simply the product of the population and an intrinsic annihilation rate. Although the annihilation spectrum contains no direct spatial information, the solution to the positron transport equations yields the time development of the different populations. The measured annihilation rate is then

$$N(t) = \lambda n_b(t) + \lambda_s n_s(t) + \lambda_{ps} n_{ps}(t) \tag{4}$$

where the subscripts b, s and ps refer to free thermal (bulk) positrons, those trapped in the surface state and para-positronium (p-Ps), respectively. The other surface processes can be neglected; ortho-positronium (o-Ps) will travel too far, within its 142 ns lifetime, to be detected and, in the absence of electrons, free positrons do not annihilate.

Of the three populations, only the bulk can be obtained directly from the solution to the positron diffusion equation, by simple integration of the thermal positron distribution over all space. In practice, if epithermal transport is also included, it is more convenient to solve for this term in the same manner as for the Ps and surface-state populations. Rate equations for the different process can be constructed as for bulk lifetime experiments. Considering only the surface state, the total rate of change is equal

to the difference between the partial sink rate out of the bulk and the annihilation from the surface state. Therefore,

$$dn_s/dt = -\lambda_s n_s(t) + (\varepsilon_s/\varepsilon)\kappa_\varepsilon(t) + (\nu_s/\nu)\kappa_\theta(t). \tag{5}$$

Equation (5) has a similar form to the usual kinetic rate equations which describe positron trapping in solids, with the important difference that the thermal and epithermal sink rates κ_θ and κ_ε are time-dependent functions which derive directly from the solutions to the respective transport equations. The partial absorption coefficients ε_s and ν_s determine the branching ratios to the different channels. Similar equations can be constructed for the bulk and p-Ps states. Neglecting thermally activated desorption of trapped positrons as Ps [2], the rate equation for Ps annihilation has an identical form with equation (5). At room temperature, desorption is usually negligible, but when present should be easily seen as a reduction in the effective surface-state lifetime.

3. Effect of an imperfectly absorbing surface

Thermal positrons have kinetic energies (relative to the crystal zero) much smaller than the surface potential barrier and are expected to have a limited probability for both escape and Ps formation, because of reflection of the positron wavefunction [1]. In this case a radiative boundary condition to the diffusion equation, describing the sink rate as proportional to the concentration at the surface,

$$D\,(\partial u/\partial z)|_{z=0} = \nu u(0, t) \tag{6}$$

is necessary. The absorption coefficient ν is directly related to the quantum mechanical transmission coefficient of the positron wavefunction and should therefore vanish as the temperature approaches zero. Such a reduction has been experimentally observed [8], in agreement with the solution of Nieminen and Oliva [1] for the time-averaged back diffusion probability:

$$J = \frac{\nu}{\nu + L\lambda}\int_0^\infty P(z)\exp\left(-\frac{z}{L}\right)dz. \tag{7}$$

The time-dependent diffusion equation (equation (1)) is best solved by a Green function method. For a radiative boundary condition and an initial distribution, the Green function for a source at depth x is [10]

$$G(z|x, t) = \frac{\exp(-\lambda t)}{\sqrt{4\pi Dt}}\left\{\exp\left(-\frac{(z-x)^2}{4Dt}\right) + \exp\left(-\frac{(z+x)^2}{4Dt}\right)\right.$$

$$\left. - \frac{2\nu}{D}\exp\left(\frac{\nu x}{D}\right)\int_{-\infty}^{x}\exp\left[-\left(\frac{(z-\eta)}{4Dt} - \frac{\nu\eta}{D}\right)\right]d\eta\right\}. \tag{8}$$

Excluding the integral and bulk annihilation term, this is the Green function G_r for

the non-decaying diffusion equation with Neumann boundary conditions (perfectly reflecting surface). Hence equation (8) can be rewritten as

$$G(z|x,t) = \exp(-\lambda t)\,[G_r(z|x,t) - G_0(z|x,t)] \tag{9}$$

where G_0 integrates to

$$G_0 = (v/D)\exp[(v/D)(z+x+vt)]\,\mathrm{erfc}[(z+x+2vt)/\sqrt{4Dt}]. \tag{10}$$

The solution to the diffusion equation, for an initial distribution $P(x)$, is then given by the integral

$$u(z,t) = \exp(-\lambda t)\int_0^\infty P(x)[G_r(z|x,t) + G_0(z|x,t)]\,\mathrm{d}x. \tag{11}$$

For the Gaussian derivative implantation profile,

$$P(x) = (2x/x_0^2)\exp(-x^2/x_0^2) \tag{12}$$

the term involving G_0 is not analytically integrable. However, for typical room-temperature values of D and v of 1 $\mathrm{cm^2\,s^{-1}}$ [11] and 10^5 $\mathrm{cm\,s^{-1}}$ [12, 13], the argument of the complementary error function is always large. Therefore it can be replaced with the asymptotic limit $\lim_{y\to\infty}[\mathrm{erfc}(y)] = [\exp(-y^2)]/y\sqrt{\pi}$, resulting in the Green function

$$G(z|x,t) = [\exp(-\lambda t)/\sqrt{4\pi Dt}]\{\exp[-(z-x)^2/4Dt] - \exp[-(z+x)^2/4Dt] + \{2(z+x)/[(z+x)+2vt]\}\exp[-(z+x)^2/4Dt]\}. \tag{13}$$

On the assumption that, for a strongly absorbing surface, within the time interval measured vt is large, the approximate Green function can be written as

$$G(z|x,t) \simeq \exp(-\lambda t)\,\{G_a(z|x,t) + [(z+x)/vt\sqrt{4\pi Dt}] \times \exp[-(z+x)^2/4Dt]\} \tag{14}$$

where G_a represents the first two terms in equation (13) and is the Green function for a perfectly absorbing surface (Dirichlet boundary conditions).

Calculating the sink rate at the surface by differentiation of $G(z|x,t)$ yields

$$D\,(\partial G/\partial z)|_{z=0} \simeq vG(0|x,t)[1 + (D/vx)(1 - x^2/2Dt)]. \tag{15}$$

From equation (15) it can be seen that internal reflection at the surface can be neglected if $vx \gg D$. This condition is simply a statement that transmission through the surface is limited by diffusion for deeply implanted positrons and by the transition rate for shallow implantation. It is not obvious, and certainly an important consideration, as to whether this is satisfied in any experimental measurement. Using the above values of v and D, as typical ambient-temperature values, the limiting depth is 1000 Å. In many cases, therefore, the effects of finite surface transmission can be neglected. As discussed in the next section, the simple diffusion model no longer applies for positrons implanted at shallower depths because many positrons return to the surface before thermalizing.

However, the above inequality was estimated for positrons implanted at a fixed depth x. For a distributed implantation profile ((equation (12)), x can, in principle, be replaced by the range x_0, but a large fraction of the distribution is nearer the surface. This will have the effect of increasing the limiting range, beyond which reflection can be ignored, for a given absorption coefficient.

To obtain a quantitative measure of the effect of finite transmission, the diffusion–annihilation equations have also been solved numerically using a finite-element method.

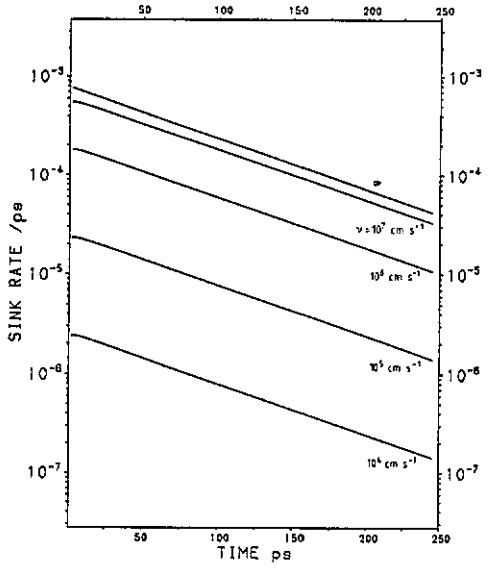

Figure 1. The total sink rate through the surface for positrons implanted at a range of 5000 Å for different values of the surface absorption coefficient ν. The curve marked ∞ is the analytical solution for a perfectly absorbing surface. Typical values of 1 cm^2 s^{-1} and 100 ps were used for the diffusion coefficient and bulk lifetime, respectively.

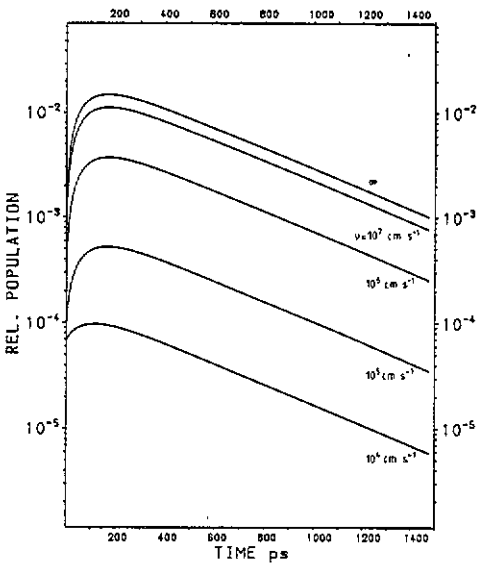

Figure 2. The surface population for positrons implanted at a range of 5000 Å for different values of the surface absorption coefficient ν. The curve marked ∞ is the analytical solution for a perfectly absorbing surface. Typical values of 1 cm^2 s^{-1}, 100 ps and 450 ps were used for the diffusion coefficient, bulk lifetime and surface lifetime, respectively. The branching ratio to the surface state was held constant at $\frac{1}{4}$.

A detailed description of the computer program will be published elsewhere. Except for the absorption coefficient ν, typical value for the positron parameters were used (see figure captions for exact values). Figure 1 shows the total sink rate through the surface for the Gaussian derivative profile (equation (12)) and a mean implantation depth x_0 of 5000 Å (corresponding to a beam energy of about ~8.5 keV in Al or 17.5 keV in Cu) for different values of ν. The curve marked ∞ is the analytical solution for a perfectly absorbing surface. For $\nu = 10^5$ cm s^{-1} the sink rate is approximately 30 times lower than for the perfect absorber, although all the curves have a similar form. Even for an absorption coefficient 100 times greater, there is still a noticeable difference. However, the apparently simple scaling is qualitatively in agreement with the analytical result for the time-averaged back diffusion probability (equation (7)). The scaling carries over into the surface-state population (figure 2), which in all cases has the same form, increasing at short times to a maximum as positrons diffuse to the surface and then exponentially decaying with the characteristic surface-state lifetime. The time at which the population is at a maximum is mainly dependent on the initial depth and annihilation rate, and only weakly on the absorption coefficient ν. The total annihilation rate, as calculated from equation (4) is shown in figure 3. In all cases, the p-Ps and bulk components mix, resulting in an annihilation spectrum which resembles a sum of two exponential components, with the surface absorption coefficient having a noticeable effect on the intensity of the longer component. However, for two different reasons, the

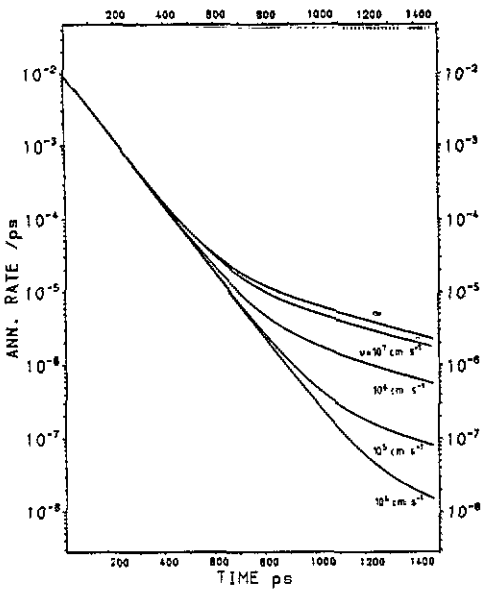

Figure 3. The total annihilation rate for positrons implanted at a range of 5000 Å for different values of the surface absorption coefficient ν. The curve marked ∞ is the analytical solution for a perfectly absorbing surface. Typical values of 1 $cm^2 s^{-1}$, 100 ps, 450 ps and 125 ps were used for the diffusion coefficient, bulk, surface and p-Ps lifetimes, respectively. The branching ratios to the surface state and p-Ps were held constant at $\frac{1}{4}$ and $\frac{1}{2}$, respectively.

intensity of the second component is not simply related to the time-averaged back-diffusion probability. Firstly, a significant fraction of the implanted positrons, which ecape as o-Ps or free positrons, does not contribute to the measured annihilation rate. Also the short component is a mixture of the diffusion determined bulk annihilation rate and the annihilation of the positrons which reach the surface and form p-Ps.

4. Epithermal and thermal positron transport

In a typical experiment, positrons are implanted mono-energetically into a sample and are assumed to achieve instantaneously a spatial distribution corresponding to the implantation profile $P(z)$ and a thermal energy distribution. This is obviously unrealistic, although for deep implantation the assumption is valid as thermalization occurs in a much shorter time than trapping or annihilation. However, at low implantation energies, the simple diffusion model does not adequately describe the experimental time-independent results. Huomo *et al* [9] explained this in terms of positrons returning to the surface before thermalizing and showed that better agreement could be obtained by simply excluding the low-energy data points in fitting the energy profile. In an early attempt to model the data, Britton and Rice-Evans [14] introduced, *ad hoc*, a second characteristic length for epithermal transport but wrongly attributed it to the elastic mean free path. Recently Kong and Lynn [15] have developed a time-independent transport model including epithermal positrons. Starting from the Boltzmann equation, they derived both an effective epithermal diffusion coefficient and a thermalization length which is approximately the *inelastic* mean free path for positron–phonon scattering.

Energetic positrons rapidly slow down, by electron scattering, to epithermal energies (a few electronvolts), below which they are only able to lose their remaining energy through inelastic scattering with phonons. As the scattering rates and mean energy loss

are very much lower, the final stages of thermalization last considerably longer than the initial stages. Consequently, in a better approximation, the implantation profile can be regarded as the initial spatial distribution of the epithermal positrons. In Monte Carlo calculations, Valkealahti and Nieminen [4] found very little difference in the range and spread of the implantation profile with end-point energy.

In a rigorous treatment, the positron diffusion equation should be solved for the initial spatial and energy distributions of the epithermal positrons including an energy-dependent diffusion coefficient and energy-dependent trapping rates at the surface. However, none of these energy dependences is known accurately, and furthermore the dependences are almost certainly strongly material dependent. Hence, a detailed treatment would have little validity and would be unnecessarily complicated. The simplest general model, which should illustrate the essential features of unthermalized positron escape from the sample, is a two-flux model, in which the epithermal positron distribution is the time-dependent source of thermal positrons.

This paper follows the method of Kong and Lynn [15] for the time-independent solution, by assuming an energy-averaged epithermal distribution with a single diffusion coefficient $D_\varepsilon = v_\varepsilon L_\varepsilon$, where v_ε is the positron velocity (about 10^5 m s^{-1}) and L_ε is the thermalization length (about 100 Å). As the thermalization rate γ is very much greater than the bulk annihilation rate λ, annihilation of epithermal positrons can be neglected and the decay term in the time-dependent diffusion equation (equation (1)) can be replaced by the thermalization rate. The diffusion equation is then solved for the epithermal distribution and the sink rate of epithermal positrons at the surface, using the usual implantation profile as the initial distribution and Dirichlet boundary conditions. Epithermal positrons have a relatively high momentum, and hence reflection at the surface can be assumed to be negligible. For simplicity, Dirichlet boundary conditions will also be applied to the thermal positron diffusion equation.

The epithermal distribution can now be included as a time-varying source in the solution for the thermal distribution. This has a similar form to the original implantation profile, except that the mean depth increases as $\sqrt{4D_\varepsilon t}$. Assuming an absorbing surface, the relevant Green function is

$$u_\varepsilon(z, t) = \{[x_0 \exp(-\gamma t)]/\sqrt{x_0^2 + 4D_\varepsilon t}\}\,[2z/(x_0^2 + 4D_\varepsilon t)] \times \exp[-z^2/(x_0^2 + 4D_\varepsilon t)]. \tag{16}$$

Differentiating at the surface yields the total epithermal sink rate

$$\kappa_\varepsilon(t) = [2D_\varepsilon x_0/(x_0^2 + 4D_\varepsilon t)^{3/2}] \exp(-\gamma t). \tag{17}$$

The epithermal distribution can now be included as a time-varying source in the solution for the thermal distribution. This has a similar form to the original implantation profile, except that the mean depth increases as $\sqrt{4D_\varepsilon t}$. Assuming an absorbing surface, the relevant Green function is

$$G(z|x, t|\tau) = [\![\{\exp[-\lambda(t-\tau)]\}/\sqrt{4\pi D_\theta(t-\tau)}]\!]\,\{\exp[-(z-x)^2/4D_\theta(t-\tau)] - \exp[-(z+x)^2/4D_\theta(t-\tau)]\} \tag{18}$$

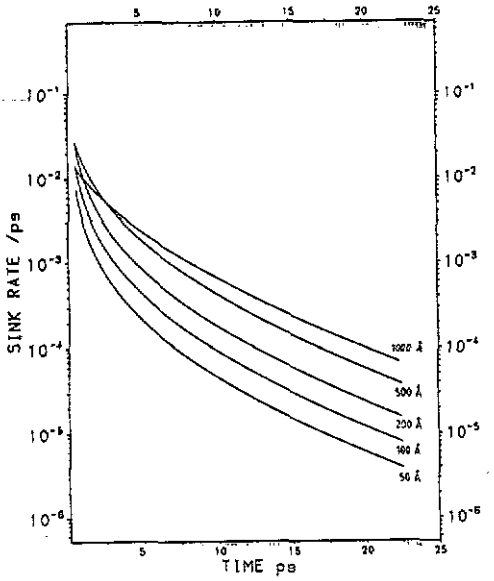

Figure 4. The total sink rate of epithermal positrons to the surface for positrons implanted epithermally at different ranges. A thermalization time of 10 ps and diffusion coefficient of 10 $cm^2 s^{-1}$ were used. The surface was assumed to be a perfect sink for epithermal positrons.

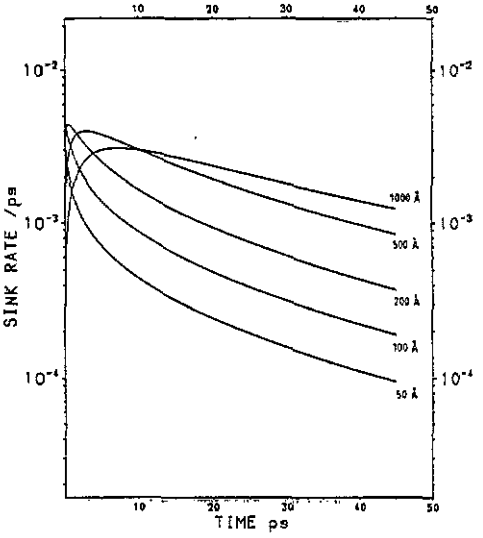

Figure 5. The total sink rate of thermal positrons to the surface for positrons implanted epithermally at different ranges. A thermalization time of 10 ps and a bulk lifetime of 100 ps were used. Diffusion coefficients of 10 $cm^2 s^{-1}$ and 1 $cm^2 s^{-1}$ for epithermal and thermal positrons, respectively, were used. The surface was assumed to be a perfect sink for all positrons.

where D_θ is the thermal positron diffusion coefficient. The thermal distribution is calculated from the double integral

$$u_\theta(z, t) = \int_0^t \int_0^\infty g(z|x, t|\tau)\gamma u_\varepsilon(x, \tau)\, dx\, d\tau \tag{19}$$

leading, eventually to the thermal sink rate

$$\begin{aligned}\kappa_\theta(t) = [x_0 D_\theta \gamma/(D_\varepsilon - D_\theta)]\{[\exp(-\lambda t)]/\sqrt{x_0^2 + 4D_\theta t} - [\exp(-\gamma t)]/\sqrt{x_0^2 + 4D_\varepsilon t} \\ + \exp(-\lambda t)\sqrt{\pi(\gamma - \lambda)/4(D_\varepsilon - D_\theta)} \\ \times \exp[(\gamma - \lambda)(x_0^2 + 4D_\theta t)/4(D_\varepsilon - D_\theta) \\ \times \{\operatorname{erf}[\sqrt{(\gamma - \lambda)(x_0^2 + 4D_\theta t)/4(D_\varepsilon - D_\theta)}] \\ - \operatorname{erf}[\sqrt{(\gamma - \lambda)(x_0^2 + 4D_\varepsilon t)/4(D_\varepsilon - D_\theta)}]\}\}.\end{aligned} \tag{20}$$

The two calculated sink rates κ_ε and κ_θ are shown in figures 4 and 5, respectively, for different positron ranges, using reasonable values for the different parameters. Typical metal values of 100 ps and 1 $cm^2 s^{-1}$ have been used for λ^{-1} and D_θ. A relatively long thermalization time $\gamma^{-1} = 10$ ps has been chosen and D_ε has been estimated as 10 $cm^2 s^{-1}$ from the definition given previously. After 10 ps, which is typically within the first channel of a positron lifetime spectrum, the epithermal sink rate is an order of magnitude

lower than the thermal sink rate. Furthermore, it is very rapidly reduced, by more than four orders of magnitude in the first 50 ps. Both of these observations suggest that, even for shallow implantation, epithermal effects are unlikely to be significant in a typical experiment.

The populations contributing to the lifetime spectrum can then be calculated from the sink rates κ_ε and κ_θ by solving the appropriate rate equations. The bulk (free thermal) population is calculated from the equation

$$n_b(t) = -\lambda n_b(t) + \gamma n_\varepsilon(t) - \kappa_\theta(t) \tag{21}$$

where $n_\varepsilon(t)$ is the spatial integral of equation (16) or the solution to the rate equation

$$n_\varepsilon(t) = -\gamma n_\varepsilon(t) - \kappa_\varepsilon(t). \tag{22}$$

Both have, obviously, the same solution

$$n_\varepsilon(t) = (x_0/\sqrt{x_0^2 + 4D_\varepsilon t}) \exp(-\gamma t) \tag{23}$$

which can be substituted into the solution for the bulk population

$$n_b(t) = \exp(-\gamma t) \int_0^\infty \exp(\lambda\tau)[\gamma n_\varepsilon(\tau) - \kappa_\theta(\tau)]\, d\tau. \tag{24}$$

The bulk population, as a function of time, for different values of the positron range x_0 is shown in figure 6. For comparison, solutions to purely thermal diffusion (broken curves) are also shown. These are given by equation (23) with a substitution of D_θ and λ for D_ε and γ. Apart from a depletion at short times, due to a finite thermalization time, the two calculations are very similar for deeply implanted positrons. Even for an implantation depth of 50 Å, the two curves merge within 250 ps, becoming a simple exponential with a decay rate equal to the bulk annihilation rate.

The surface, and p-Ps, populations are given by the solution equation (5):

$$n_s(t) = \exp(-\lambda_s t) \int_0^\infty \exp(\lambda_s \tau) \left(\frac{\varepsilon_s}{\varepsilon} \kappa_\varepsilon(\tau) + \frac{\nu_s}{\nu} \kappa_\theta(\tau) \right) d\tau \tag{25}$$

with an appropriate substitution of the Ps parameters for the p-Ps population. The three different populations are shown, along with the total annihilation rate, in figure 7 for positrons implanted at 1000 Å. As before, the broken curves show the solution without epithermal corrections. The greatest difference is in the surface-state population. Although the transport of epithermal positrons to the surface occurs within a very short time after implantation, those that are trapped in the surface state are very long lived and the cumulative effect is still noticeable after hundreds of picoseconds. Another noticeable effect of the early occupancy of the surface state by unthermalized positrons is a shift to shorter times of the maximum population.

The total annihilation rate is shown for different positron ranges in figure 8. To enhance clarity the curves have been successively scaled by a factor of 5 and hence only the lowest pair (5000 Å) shows the actual calculated annihilation rate. Two effects can be clearly seen. Firstly, as expected from the surface population, epithermal positrons reaching the surface increase the intensity of the longer component. This is most clearly seen for deeper implantations, when the intensity is lower, although the absolute change is in all cases about 3%. Secondly, probably because of epithermals feeding the p-Ps state which contributes a constant decay rate to the shorter component, the shorter component is slightly longer lived. The reduction in annihilation rate at very short times

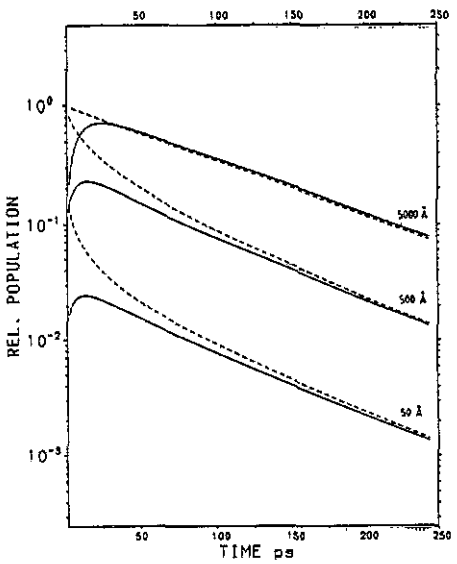

Figure 6. The bulk population of thermal positrons implanted epithermally (——) and thermally (----) at different ranges. A thermalization time of 10 ps and a bulk lifetime of 100 ps were used. Diffusion coefficients of 10 $cm^2 s^{-1}$ and 1 $cm^2 s^{-1}$ for epithermal and thermal positrons, respectively, were used. The surface was assumed to be a perfect sink for all positrons.

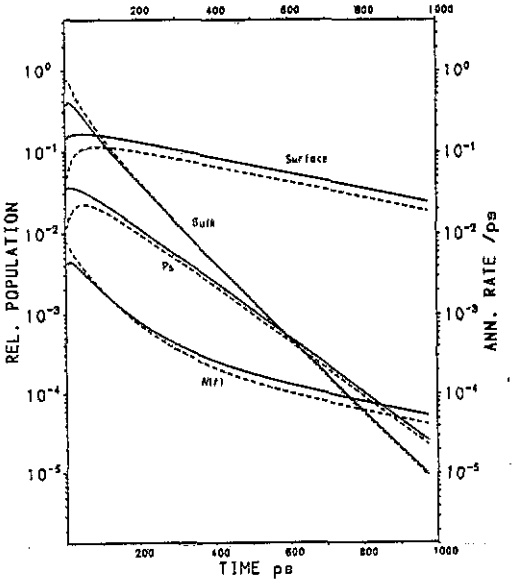

Figure 7. Calculated populations of the p-Ps, surface-trapped and free-thermal-positron states for positrons implanted epithermally (——) and thermally (----) with a range of 1000 Å. A thermalization time of 10 ps and a bulk lifetime of 100 ps were used. Diffusion coefficients of 10 $cm^2 s^{-1}$ and 1 $cm^2 s^{-1}$ for epithermal and thermal positrons, respectively, were used. Lifetimes of 450 ps and 125 ps were used for the surface state and p-Ps, respectively. Branching ratios to the surface state and p-Ps were held constant at $\frac{1}{4}$ and $\frac{1}{3}$ for both thermal and epithermal positrons. The surface was assumed to be a perfect sink for all positrons. $N(t)$ is the total annihilation rate, resulting from a weighted superposition of the three components.

is an artefact of the assumption that unthermalized positrons do not annihilate and indicates the finite thermalization rate.

5. Conclusions

Annihilation spectra, resulting from the implantation of mono-energetic positrons into a perfect homogeneous solid, have been modelled using typical ambient-temperature parameter values. The resulting curves can be reasonably well described as a sum of two exponential components, although the intensities are not simply related to the time-averaged positron back diffusion probability. The longer component is, in the absence of thermal desorption, simply the annihilation rate of positrons trapped in the surface potential. Free-positron and p-Ps annihilations constitute the shorter component.

The effects of epithermal positrons reaching the surface and of internal reflection of thermal positrons have been considered. Epithermal effects, even at shallow depths,

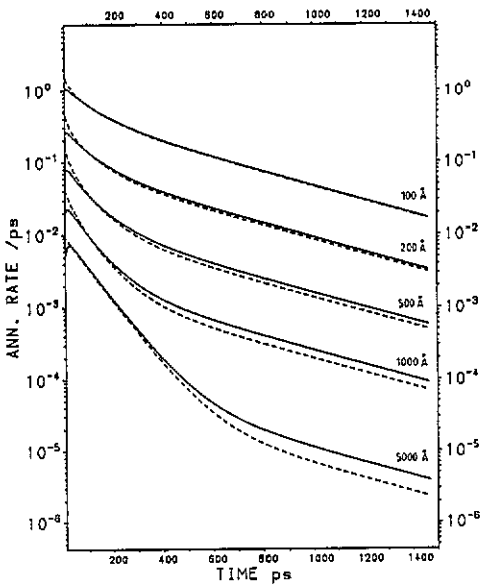

Figure 8. Relative annihilation rates, calculated using the previous parameter values for different ranges of the implantation profile: ——, epithermal implantation; – – – –, thermal implantation. Successive curves, in order of decreasing depth, have been scaled by a factor of 5 to present a clearer picture.

are less significant than for time-independent measurements because of the relative short times involved in the epithermal transport processes, the main effect being an increase in the longer component by a few per cent of the total intensity. The lifetime of the shorter component is also increased because of mixing with the constant 125 ps p-Ps annihilation lifetime.

At room temperature, internal reflection of thermal positrons can be neglected for deep source profiles. In practice, because of the rapid escape of unthermalized positrons from the near-surface region, all thermal sources can be considered as deep. Using the values in the text, the mean depth of the thermal source increases as $\sqrt{4D_+t}$ (equation (16)), typically 2000 Å in 10 ps. This is not the case, however, at low temperatures as the surface absorption coefficients vanish at zero temperature. A numerical solution with radiative boundary conditions appears to show a relatively simple scaling of the sink rates, similar to behaviour of the back-diffusion probability in the time-independent case.

Acknowledgments

I am grateful to Gottfried Kögel, Risto Nieminen and Kjeld Jensen for useful discussions.

References

[1] Nieminen R M and Oliva J 1980 *Phys. Rev.* B **22** 2226
[2] Schultz P J and Lynn K G 1989 *Rev. Mod. Phys.* **60** 701
[3] Vehanen A, Saarinen K, Hautojärvi P and Huomo H 1987 *Phys. Rev.* B **35** 4606
[4] Valkealahti S and Nieminen R M 1984 *Appl. Phys.* A **35** 51
[5] Schödlbauer D, Sperr P, Kögel G and Triftshäuser W 1988 *Nucl. Instrum. Methods* B **34** 258
[6] Lynn K G, Frieze W E and Schultz P J 1988 *Phys. Rev. Lett.* **52** 1137

[7] Frieze W E, Lynn K G and Welch D O 1985 *Phys. Rev.* B **31** 15
[8] Britton D T, Huttunen P A, Mäkinen J, Soininen E and Vehanen A 1989 *Phys. Rev. Lett.* **62** 2413
[9] Huomo H, Vehanen A, Bentzon M D and Hautojärvi P 1987 *Phys. Rev.* B **35** 8252
[10] Sommerfeld A 1978 *Theoretische Physik* vol 6, 6th edn (Frankfurt: Harri Deutsch)
[11] Soininen E, Huomo H, Huttunen P A, Mäkinen J, Hautojärvi P and Vehanen A 1990 *Phys. Rev.* B **41** 6227
[12] Jensen K O, Eldrup M, Linderoth S and Evans J H 1990 *J. Phys.: Condens. Matter* **2** 2081
[13] Huttunen P A, Mäkinen J, Britton D T, Soininen E and Vehanen A 1990 *Phys. Rev.* B **42** 1560
[14] Britton D T and Rice-Evans P C 1988 *Phil. Mag. Lett.* **57** 165
[15] Kong Y and Lynn K G 1990 *Phys. Rev.* B **41** 6179